Polymer 50 (2009) 6186–6191

Contents lists available at ScienceDirect

Polymer

journal homepage: www.elsevier.com/locate/polymer

Performance inhomogeneity of gelatin during gelation process

Xiliang Chen [a], Yuxi Jia [a,*], Sheng Sun [a], Ligang Feng [a], Lijia An [b,*]

[a] School of Materials Science & Engineering, Shandong University, Jinan 250061, China
[b] State Key Laboratory of Polymer Physics and Chemistry, Changchun Institute of Applied Chemistry, Chinese Academy of Sciences, Changchun 130022, China

ARTICLE INFO

Article history:
Received 16 May 2009
Received in revised form
20 September 2009
Accepted 12 October 2009
Available online 22 October 2009

Keywords:
Performance inhomogeneity
Gel point
Equilibrium shear modulus

ABSTRACT

The structural and performance inhomogeneities of gelatin gel can directly affect its application as a kind of functional material. The structural inhomogeneity of gelatin caused by the uneven and unstable temperature field has been analyzed by the finite element method in our previous work. Further in this paper, the performance inhomogeneity of gelatin which is closely connected with the actual application is numerically analyzed during the gelation process, which includes the inhomogeneities of the optical and mechanical properties of gelatin gels. The time required for reaching the gel point at different spatial grids is exhibited and discussed. The calculated results also show that the equilibrium shear modulus of gelatin is dependent on the thermal history.

1. Introduction

The inhomogeneity of polymer gels has been widely concerned by researchers. On the one hand, the inhomogeneity may be a kind of product defect if homogenous gels are required. On the other hand, the inhomogeneity can be well utilized to achieve special functions. For example, a kind of polymer gel with an internally heterogeneous or modulated structure has shape memory properties [1]; some inhomogenous hydrogels can form patterned area on the surface, and the surface patterning techniques may be used in display and sensor fields [2].

As a kind of functional material, gelatin gel is widely used in medical, pharmaceutical, food preparation, photographic and holographic industries [3–7]. The structural and performance inhomogeneities of gelatin products can directly affect their applications. For instance, in photographic industries, the inhomogeneity of gelatin can affect its refractive index [8]. As a drug carrier, a gelatin gel with nonuniform degrees of crosslinking can adjust the rate of the drug release [9].

As mentioned in Ref. [10], the low thermal conductivity of gelatin can lead to the uneven and unstable temperature field, which further results in the structural and performance inhomogeneities during the gelation process. The dynamic gelation process makes it difficult to measure the structural and performance parameters in time and space scales in experiments. Hence, the computer simulation has been used to analyze the gelation process of gelatin [10–13].

The finite element method has been used in the study of both chemical [14–18] and physical [10,19–21] gelation processes. In our previous work [10], the structural inhomogeneity of gelatin caused by the uneven and unstable temperature field has been analyzed by the finite element method. But the study on the performance inhomogeneity of gelatin caused by the complicated temperature field is relatively rare by now. So in this paper, the performance inhomogeneity of gelatin is analyzed, which includes the inhomogeneities of the specific optical rotation, the gel point, the viscosity below the gel point and the modulus beyond the gel point. The present work is helpful for optimizing the fabrication conditions of gelatin.

2. Numerical calculation of key parameters

2.1. Numerical calculation of reverted helix fraction

The sol–gel transition of gelatin is induced by the coil–helix reversion when the temperature is reduced to a certain value. The numerical calculating equations of the reverted helix fraction have been presented in our previous work [10] as follows.

In the first time step Δt when the reversion starts, the reverted fractions of single-looped and nonlooped triple helices, $X_{1(1)}$ and $X_{2(1)}$ is calculated as [10]

$$X_{1(1)} = -\frac{a_{(1)}^2\theta_{(1)}\Delta t}{b_{(1)}\varphi} + \frac{a_{(1)}}{b_{(1)}\varphi}\ln\left(\frac{\left(a_{(1)}\theta_{(1)}+b_{(1)}\varphi\right)\exp\left(a_{(1)}\theta_{(1)}\Delta t\right)-b_{(1)}\varphi}{a_{(1)}\theta_{(1)}}\right) \quad (1)$$

* Corresponding authors. Tel.: +86 531 88395811; fax: +86 431 85262206.
E-mail addresses: jia_yuxi@sdu.edu.cn (Y. Jia), ljan@ciac.jl.cn (L. An).

0032-3861/$ – see front matter © 2009 Elsevier Ltd. All rights reserved.
doi:10.1016/j.polymer.2009.10.027

$$X_{2(1)} = \frac{1}{\varphi}\left(1+\frac{a_{(1)}^2\theta_{(1)}^2\Delta t}{b_{(1)}\varphi}-\frac{a_{(1)}\theta_{(1)}}{\left(a_{(1)}\theta_{(1)}+b_{(1)}\varphi\right)\exp\left(a_{(1)}\theta_{(1)}\Delta t\right)-b_{(1)}\varphi}\right) - \frac{a_{(1)}\theta_{(1)}}{b_{(1)}\varphi}\ln\left(\frac{\left(a_{(1)}\theta_{(1)}+b_{(1)}\varphi\right)\exp\left(a_{(1)}\theta_{(1)}\Delta t\right)-b_{(1)}\varphi}{a_{(1)}\theta_{(1)}}\right) \quad (2)$$

where the subscript (1) denotes being in the first time step, b the parameter determined by the gelatin temperature and concentration, a and θ the parameter determined by the temperature only, φ the constant.

At the time of $n\Delta t (n \geq 2)$, the reverted helix fractions, $X_{1(n)}$ and $X_{2(n)}$, are obtained by means of backward difference method and incremental method [10]

$$X_{1(n)} = a_{(n)}\Delta t\left(1-\theta_{(n)}X_{1(n-1)}-\varphi X_{2(n-1)}\right)+X_{1(n-1)} \quad (3)$$

$$X_{2(n)} = b_{(n)}\Delta t\left(1-\theta_{(n)}X_{1(n-1)}-\varphi X_{2(n-1)}\right)^2+X_{2(n-1)} \quad (4)$$

where the subscript $(n-1)$ denotes being at the time of $(n-1)\Delta t$.

The total reverted helix fraction $X_{(n)}$ is [10]

$$X_{(n)} = X_{1(n)}+X_{2(n)} \quad (5)$$

2.2. Numerical calculation of specific optical rotation

Optical rotation is the property displayed by chiral substances of rotating the plane of polarisation of polarized light. And for gelatin, the optical rotation is an important physical property which is helpful for measuring the reverted helix fraction in experiments. Gelatin is levorotary, and its optical rotation is negative by definition [22,23]. The specific optical rotation is defined as follows

$$[\alpha]_\lambda = \frac{100\alpha}{lc} \quad (6)$$

where α denotes the optical rotation measured at the wavelength λ when the light beam passes the length of l (in decimeters), c (in grams per deciliter) the gelatin concentration.

The reverted helix fraction of gelatin is closely associated with the specific optical rotation, and is presented as [22,23]

$$X = \frac{[\alpha]_\lambda-[\alpha]_\lambda^{\text{coil}}}{[\alpha]_\lambda^{\text{collagen}}-[\alpha]_\lambda^{\text{coil}}} \quad (7)$$

where X denotes the reverted helix fraction, $[\alpha]_\lambda$ the measured specific optical rotation, $[\alpha]_\lambda^{\text{coil}}$ the specific optical rotation if all gelatin molecules are in the coil state, $[\alpha]_\lambda^{\text{collagen}}$ the specific optical rotation if all gelatin molecules are in the helix state, namely the same as the native state of collagen.

The numerical calculating equation of the specific optical rotation of gelatin can be obtained by Eq. (7)

$$[\alpha]_\lambda = X_{(n)}\left([\alpha]_\lambda^{\text{collagen}}-[\alpha]_\lambda^{\text{coil}}\right)+[\alpha]_\lambda^{\text{coil}} \quad (8)$$

Through a series of experimental studies, Djabourov et al. [24] found that the mass concentration of the triple helix reaches a certain value at the gel point of gelatin. Then van der Linden and Parker [25] supplemented this statement, and presented the critical helix volume fraction $f_c = 0.0028$. The density of gelatin has been measured by researchers and is equal to 1.44 g/cm^3 [24]. Thereby, the reverted helix fraction at the gel point is calculated as

$$X_{\text{gel}} = \frac{0.4032}{c} \quad (9)$$

where the gelatin concentration c is in grams per deciliter.

According to Eqs. (8)–(9), the specific optical rotation of gelatin at the gel point is obtained as

$$[\alpha]_\lambda^{\text{gel}} = \frac{0.4032\left([\alpha]_\lambda^{\text{collagen}}-[\alpha]_\lambda^{\text{coil}}\right)}{c}+[\alpha]_\lambda^{\text{coil}} \quad (10)$$

Colby et al. [26] studied the specific optical rotation of gelatin at the wavelength of $\lambda = 632.8$ nm, and presented that $[\alpha]_{632.8}^{\text{collagen}} = -327 \pm 5$ is almost a constant for various gelatin concentrations and temperatures. They also found that the specific optical rotation of the gelatin in the coil state $[\alpha]_\lambda^{\text{coil}}$ has a linear relationship to the temperature change [26]

$$[\alpha]_{632.8}^{\text{coil}} = 0.311T-134 \quad (11)$$

where the temperature T is in Celsius.

Thus, at the wavelength of $\lambda = 632.8$ nm, the specific optical rotation of gelatin at the gel point is obtained as a function of the gelatin concentration c and temperature T by Eqs. (10)–(11), and is expressed as

$$[\alpha]_{632.8}^{\text{gel}} = -\frac{0.4032(0.311T+193)}{c}+0.311T-134 \quad (12)$$

Because the specific optical rotation of gelatin is negative, it can be concluded from Eq. (12) that the absolute value of the specific optical rotation at the gel point decreases as the gelatin concentration increasing.

The calculated results by Eq. (12) have been compared with the experimental data presented by Colby et al. in Table 2 in Ref [27]. They are in good agreement with each other. Eq. (12) is helpful for determining the gel point precisely, nondestructively and conveniently by polarimetry measurement in experiments.

At the wavelength of $\lambda = 632.8$ nm, Eq. (8) can be rewritten as

$$[\alpha]_{632.8} = -X_{(n)}(0.311T+193)+0.311T-134 \quad (13)$$

2.3. Numerical calculation of mechanical parameters

As important physical properties, the mechanical parameters of gelatin which can directly affect the practical applications have been studied by numerous researchers [24–27].

Colby et al. [27] used the dynamic scaling theory to describe the viscosity below the gel point and the equilibrium shear modulus beyond the gel point.

The increased viscosity below the gel point is described as [27]

$$\Delta\eta = A(-\varepsilon)^{-s} \quad (14)$$

by denoting

$$\varepsilon = \left(X-X_{\text{gel}}\right)/X_{\text{gel}} \quad (15)$$

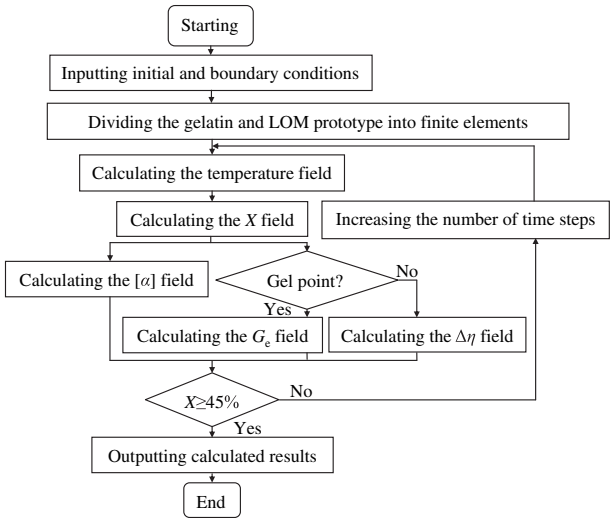

Fig. 1. Flow chart of the finite element simulation (The LOM prototype is a mold core used to provide a specific shape for the gelatin part, X denotes the reverted helix fraction, $[\alpha]$ the specific optical rotation, $\Delta\eta$ the increased viscosity below the gel point, and G_e the equilibrium shear modulus beyond the gel point).

where A denotes the prefactor determined by the gelatin temperature and concentration, and s the exponent determined by the gelatin concentration only.

The equilibrium shear modulus beyond the gel point is described as [27]

$$G_e = B\varepsilon^t \tag{16}$$

where B denotes the prefactor determined by the gelatin temperature and concentration, and t the exponent determined by the gelatin concentration only.

2.4. Governing equations of temperature field and boundary conditions

The governing equations of the temperature field and the boundary conditions have been presented in our previous work [10]. The basic equations are listed as follows.

The partial differential equation of temperature field in two-dimensional space is obtained as

$$D[T(x,y,t)] = \lambda\left(\frac{\partial^2 T}{\partial x^2}+\frac{\partial^2 T}{\partial y^2}\right) - \rho_g c_p \frac{\partial T}{\partial t} = 0 \tag{17}$$

where the coefficient of thermal conductivity λ, specific heat c_p at constant pressure and gelatin density ρ_g are regarded as constants.

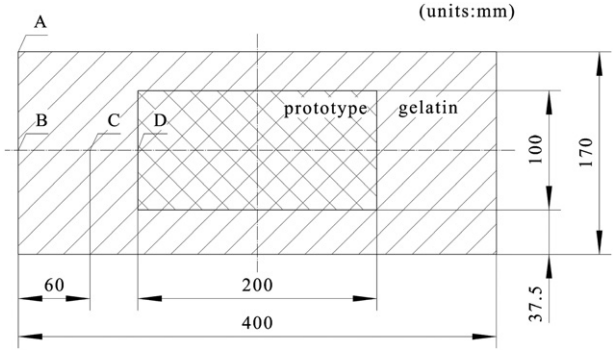

Fig. 2. Structure and dimensions of calculated example.

Table 1
Key input data.

Parameters	Numerical values
Density of gelatin system when $c_0 = 2.62$ g/dL	1008 kg/m^3
Specific heat of gelatin system	4.174 kJ/(kg K)
Coefficient of thermal conductivity of gelatin system	0.1924 W/(m K) [28]
Volume specific heat of prototype	2000 kJ/(m^3 K)
Coefficient of thermal conductivity of prototype	0.01 W/(m K)
Surface roughness of prototype	0.0001 m
Coefficient of convective heat transfer	6 W/(m^2 K)
Viscosity exponent	1.6475 [27]
Elasticity exponent	2.205 [27]

The control equation of temperature field is derived by Galerkin method

$$\iint_D \left[\lambda\left(\frac{\partial W_l}{\partial x}\frac{\partial T}{\partial x}+\frac{\partial W_l}{\partial y}\frac{\partial T}{\partial y}\right)+\rho_g c_p W_l \frac{\partial T}{\partial t}\right]dxdy - \oint_\Gamma \lambda W_l \frac{\partial T}{\partial n}ds = 0 \quad (l = 1,2,\cdots,n; j = 1,2,\cdots,m) \tag{18}$$

where W_l denotes the lth trial function, and Γ the boundary of integral area.

3. Procedures of numerical simulation

The numerical simulation procedures are shown in Fig. 1.

The same as that mentioned in Ref. [10], the effects of mass transfer process via convection and diffusion induced by temperature and concentration gradients are not taken into account in the simulation.

4. Simulated example

The shape of the sample is the same as that in Ref. [10], and is shown in Fig. 2.

The initial temperature of the example is 45 °C, located in the cold atmosphere with the temperature of 10 °C. The gelatin concentration is taken as 2.62 g/dL. Thus, the prefactors A and B can be linearly fitted as functions of gelatin temperature T from the experimental data presented by Colby et al. [27], and are expressed as

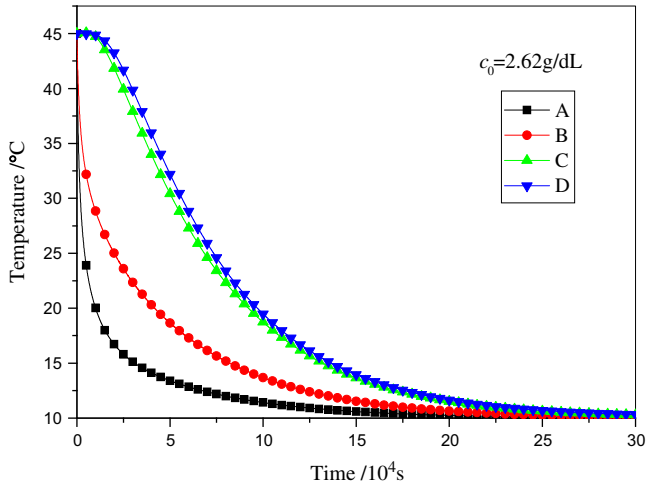

Fig. 3. Curves of gelatin temperature versus time on four different nodes.

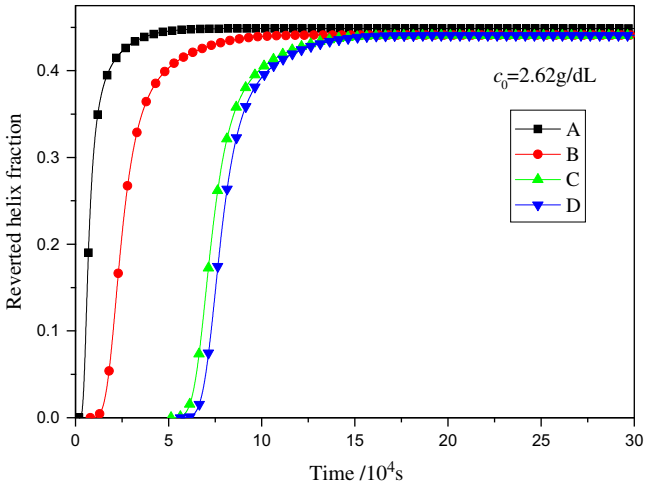

Fig. 4. Curves of reverted helix fraction versus time on four different nodes.

$$\begin{aligned} A &= 0.128T - 1.11 \\ B &= -40T + 1530 \end{aligned} \tag{19}$$

where the temperature T is in Celsius.

According to Eq. (9), when the gelatin concentration is 2.62 g/dL, the reverted helix fraction at the gel point, X_{gel}, can be calculated, which is equal to 15.39%. Hence, when the reverted helix fraction reaches 15.39%, the gel point is reached.

The main input parameters are listed in Table 1.

5. Results and discussions

5.1. Evolution of gelatin temperature

The curves of the gelatin temperature versus time are shown in Fig. 3. It can be seen that the differences of the temperature histories among nodes A, B, C, and D are obvious. In experimental studies, in order to facilitate the measurement and recording, the temperatures are usually controlled to be constant or changed at a constant rate. While the simulation results shown in Fig. 3 describe a more complex situation than that in previous experimental studies, and the former is more common in actual production process than the latter, especially when the gelatin sample is large.

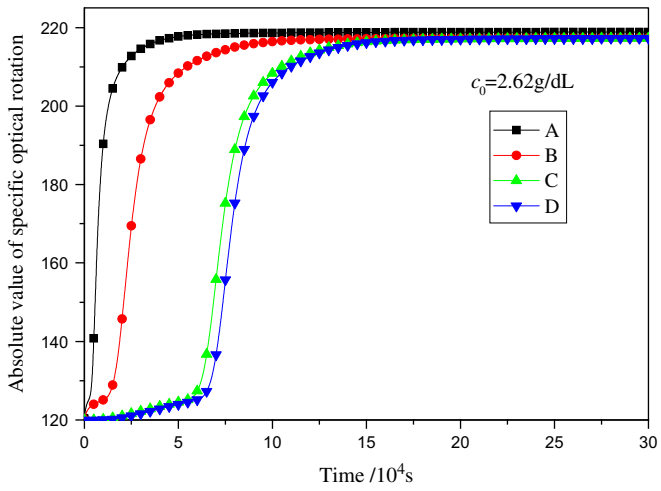

Fig. 5. Curves of specific optical rotation versus time on four different nodes.

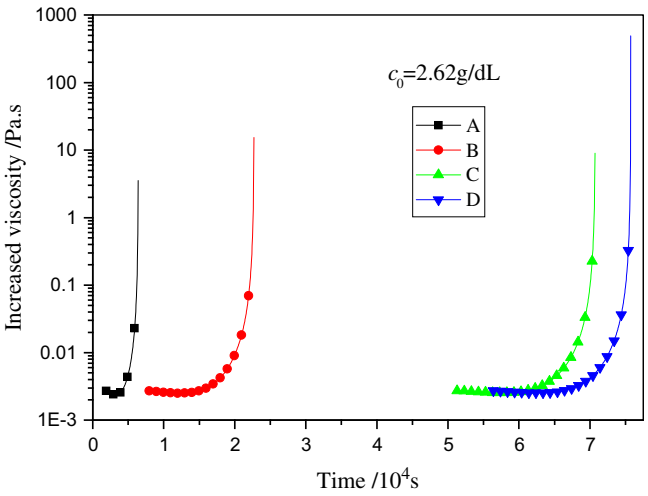

Fig. 6. Curves of increased viscosity versus time on four different nodes.

5.2. Evolution of reverted helix fraction

The curves of the reverted helix fraction versus time are shown in Fig. 4. The coil–helix transition occurs first on node A, which is followed by nodes B, C, and D. When the value of the reverted helix fraction on node A has become steady at the time of 5×10^4s, the coil–helix transition on node D has not started yet. Hence, the inhomogeneity of the reverted helix fraction of gelatin during the gelation process is obvious.

The following is the comparison between the simulation results and the experimental ones. In Ref. [29], the gelation processes of several kinds of gelatin are studied experimentally using small samples under constant cooling rate, in which the so-called "A1" gelatin is the same as the one used in this paper. Therefore, the simulation results on node A in Fig. 2 can be compared with the experimental results of the "A1" gelatin in Ref. [29]. The final temperatures of the gelatin in both simulation and experiment are all 10 °C, and the final values of the reverted helix fractions are similar. Hence, the reasonableness of the simulation results is confirmed. However, the simulation results show the inhomogeneity of the reverted helix fraction of gelatin during the gelation process, while the experimental studies not. It is necessary to analyze the inhomogeneity of some physical parameters of gelatin,

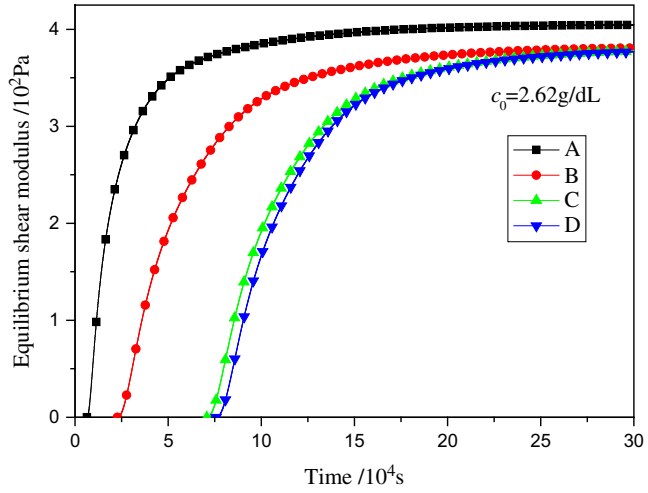

Fig. 7. Curves of equilibrium shear modulus versus time on four different nodes.

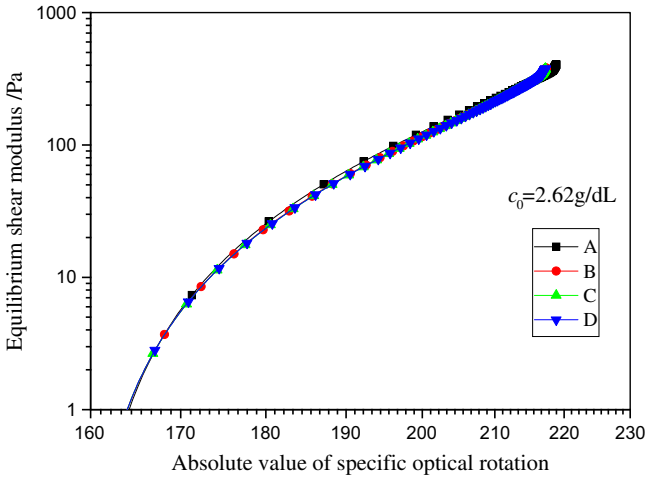

Fig. 8. Curves of equilibrium shear modulus versus specific optical rotation on four different nodes.

especially for the parameters which are dependent on the thermal histories.

5.3. Evolution of specific optical rotation

The curves of the specific optical rotation of gelatin versus time are shown in Fig. 5. From the very beginning, the change rate of the specific optical rotation on node A is larger than that on other nodes. At the time of 5×10^4s, the value of the specific optical rotation on node A has become steady, while the one on node D is still very low. Until the time of about 1.6×10^5s, the value of the specific optical rotation on node D has gotten steady. Hence, the inhomogeneity of the specific optical rotation of gelatin during the gelation process is obvious.

5.4. Evolution of increased viscosity below gel point

The curves of the increased viscosity of gelatin below the gel point versus time are shown in Fig. 6. For each node, the viscosity increases drastically at a certain time. The sudden increase of the viscosity denotes the gel point is reached at that time. Fig. 6 also shows the different gelation time on different nodes. The nodes on the surface reach the gel point earlier than the inner ones. The reason is analyzed below.

As mentioned in Section 4, when the gelatin concentration is 2.62 g/dL, the reverted helix fraction at the gel point is calculated to be equal to 15.39%. Then, in the light of Fig. 4, we can draw the conclusion that node A reaches the gel point first, followed by nodes B, C, and D.

5.5. Evolution of equilibrium shear modulus beyond gel point

The curves of the equilibrium shear modulus of gelatin beyond the gel point versus time are shown in Fig. 7. The evolution characteristics of the equilibrium shear modulus are similar to those of the reverted helix fraction shown in Fig. 4, which can be explained by the following analysis. According to Eqs. (15)–(16) and (19), the equilibrium shear modulus is a function of the reverted helix fraction and gelatin temperature at a certain gelatin concentration. But the reverted helix fraction is the principal factor that affects the equilibrium shear modulus. Hence, the evolution characteristics of the equilibrium shear modulus and the reverted helix fraction are similar.

In Fig. 7, the equilibrium shear modulus of node A is significantly higher than that of others. The phenomenon is explained below. On the ground of Eq. (16), a small change of ε can lead to a great change of the equilibrium shear modulus. And based on Eq. (15), the value of ε is determined by the reverted helix fraction. Fig. 4 shows that the reverted helix fraction of node A is a little higher than that of others, which eventually results in the much higher equilibrium shear modulus of node A than that of others.

5.6. Relation between specific optical rotation and equilibrium shear modulus

The curves of the equilibrium shear modulus of gelatin versus the specific optical rotation are shown in Fig. 8. The equilibrium shear modulus has a power growth with the absolute value of specific optical rotation, with the exponent changing from the initial 24 to the final 12. The explanation is as follows.

Colby et al. have established the relationship between the specific optical rotation and the equilibrium shear modulus by presenting that [27]

$$\varepsilon = \frac{[\alpha]_\lambda - [\alpha]_\lambda^{\mathrm{gel}}}{[\alpha]_\lambda^{\mathrm{gel}} - [\alpha]_\lambda^{\mathrm{coil}}} \tag{20}$$

At the wavelength $\lambda = 632.8$ nm and the gelatin concentration $c = 2.62$ g/dL, according to Eqs. (11)–(12) and (19)–(20), Eq. (16) can be rewritten as

$$G_e = (-40T + 1530)\left(\frac{[\alpha]_{632.8} - 0.263T + 207.664}{-0.048T - 73.664}\right)^{2.205} \tag{21}$$

Eq. (21) indicates that the equilibrium shear modulus G_e is a function of the specific optical rotation $[\alpha]_{632.8}$ and the gelatin temperature T. Hence, the growth exponent of the equilibrium shear modulus versus the specific optical rotation in Fig. 8 is affected by the gelatin temperature, and changes with the gelatin temperature changing during the whole gelation process.

6. Conclusions

The spatial performance inhomogeneity of gelatin is numerically analyzed during the cooling-induced gelation process. The surface parts of gelatin reach the gel point earlier than the inner ones. And the equilibrium shear modulus of gelatin is found to be dependent on the thermal history. The equilibrium shear modulus of the surface parts of gelatin is larger than that of the inner ones at the end of transition, and it has a basically power growth with the linear increase of the absolute value of the specific optical rotation, with the exponent changing from the initial 24 to the final 12.

The present work is helpful for optimizing gelatin fabrication conditions, and then the design of the gelation process according to certain requirements can be done.

Acknowledgements

This work is supported by the National Natural Science Foundation of China (50621302, 20734003, 20620120105) Programs.

References

[1] Hu ZB, Zhang XM, Li Y. Synthesis and application of modulated polymer gels. Science 1995;269:525–7.
[2] Hu ZB, Chen YY, Wang CJ, Zheng YD, Li Y. Polymer gels with engineered environmentally responsive surface patterns. Nature 1998;393:149–52.
[3] Young S, Wong M, Tabata Y, Mikos AG. Gelatin as a delivery vehicle for the controlled release of bioactive molecules. Journal of Controlled Release 2005;109:256–74.

[4] Olsen D, Yang CL, Bodo M, Chang R, Leigh S, Baez J, et-al. Recombinant collagen and gelatin for drug delivery. Advanced Drug Delivery Reviews 2003;55: 1547–67.
[5] Tabata Y, Ikada Y. Protein release from gelatin matrices. Advanced Drug Delivery Reviews 1998;31:287–301.
[6] Kurtz RL, Owen RB. Holographic recording materials. Optical Engineering 1975;14:393–401.
[7] Karim AA, Bhat R. Gelatin alternatives for the food industry: recent developments, challenges and prospects. Trends in Food Science & Technology 2008;19:644–56.
[8] Edward S. Local inhomogeneities in the refractive index of gelatin containing a silver image treated with a tanning bleach. Photographic Science and Engineering 1969;13:29–31.
[9] Wan YZ, Wang YL, Cheng GX, Yao KD. Preparation and characterization of gelatin gel with a gradient structure. Polymer International 2000;49:1600–3.
[10] Chen XL, Jia YX, Feng LG, Sun S, An LJ. Numerical simulation of coil–helix transition processes of gelatin. Polymer 2009;50:2181–9.
[11] Pineiro Y, Lopez-Quintela MA, Rivas J, Leisner D. Percolation threshold and scattering power law of gelatin gels. Physical Review E 2009;79:041409.
[12] Redondo YP, Quintela AL, Rivas J. MC simulation of a physical gel. Colloid and Surface A-Physicochemical and Engineering Aspects 2005;270:205–12.
[13] Abete T, Del Gado E, Serughetti DH, de Arcangelis L, Djabourov M, Coniglio A. Kinetics of bond formation in cross-linked gelatin gels. Journal of Chemical Physics 2006;125:174903.
[14] Andrade SR, Jardini AL, Maciel MRW, Maciel R. Numerical simulation of localized cure of thermosensitive resin during thermo stereolithography process (TSTL). Composites Science and Technology 2007;67:1666–73.
[15] Ellwood KRJ, Baldwin J, Bauer DR. Numerical simulation of thermal oxidation in automotive tires. Rubber Chemistry and Technology 2006;79:249–66.
[16] Ghoreishy MHR, Naderi G. Three-dimensional finite element modeling of rubber curing process. Journal of Elastomers and Plastics 2005;37:37–53.
[17] Jia YX, Sun S, Xue SX, Liu LL, Zhao GQ. Investigation of computer-aided engineering of silicone rubber vulcanizing (II)-finite element simulation of unsteady vulcanization field. Polymer 2002;43:7515–20.
[18] Jia YX, Sun S, Liu LL, Xue SX, Zhao GQ. Investigation of computer-aided engineering of silicone rubber vulcanizing (I)-vulcanization degree calculation based on temperature field analysis. Polymer 2003;44:319–26.
[19] Yang WH, Rao MA. Transient natural convection heat transfer to starch dispersion in a cylindrical container: numerical solution and experiment. Journal of Food Engineering 1998;36:395–415.
[20] Nielsen H, Marr BU, Hvidt S. Correlation between sagging and shear elasticity in pectin, gelatin and polyacrylamide gels. Carbohydrate Polymers 2001;45:395–401.
[21] Feng LG, Jia YX, Chen XL, An LJ. Finite element simulation of the physical gelation of rennet casein. Acta Polymerica Sinica 2008;(6):529–36.
[22] Hauschka PV, Harrington WF. Collagen structure in solution. III. Effect of cross-links on thermal stability and refolding kinetics. Biochemistry 1970;9: 3734–45.
[23] Djabourov M, Papon P. Influence of thermal treatments on the structure and stability of gelatin gels. Polymer 1983;24:537–42.
[24] Joly-Duhamel C, Hellio D, Ajdari A, Djabourov M. All gelatin networks: 2. The master curve for elasticity. Langmuir 2002;18:7158–66.
[25] van der Linden E, Parker A. Elasticity due to semiflexible protein assemblies near the critical gel concentration and beyond. Langmuir 2005;21:9792–4.
[26] Guo L, Colby RH, Lusignan CP, Whitesides TH. Kinetics of triple helix formation in semidilute gelatin solutions. Macromolecules 2003;36:9999–10008.
[27] Guo L, Colby RH, Lusignan CP, Howe AM. Physical gelation of gelatin studied with rheo-optics. Macromolecules 2003;36:10009–20.
[28] James HB, Wilmer LS. Thermal conductivity measurements of viscous liquids. Industrial and Engineering Chemistry 1955;47:289–93.
[29] Joly-Duhamel C, Hellio D, Djabourov M. All gelatin networks: 1. Biodiversity and physical chemistry. Langmuir 2002;18:7208–17.